Supporting information

The formation of Mg-orthocarbonate through the reaction $MgCO_3$+MgO = Mg_2CO_4 at Earth's lower mantle $P-T$ conditions

Pavel N. Gavryushkin *[1,2], Dinara N. Sagatova[1,2], Nursultan Sagatov[1], and Konstantin D. Litasov[3]

[1] *Sobolev Institute of Geology and Mineralogy, Siberian Branch of Russian Academy of Sciences, prosp. acad. Koptyuga 3, 630090 Novosibirsk, Russia*
[2] *Novosibirsk State University, Pirogova 2, Novosibirsk 630090, Russia*
[3] *Vereshchagin Institute for High Pressure Physics RAS, 108840, Troitsk, Moscow, Russian Federation*

Details of the computational methods

Crystal structure predictions. The crystal structure prediction calculations using USPEX were performed at 25, 50, and 100 GPa for 1–4 formula units per unit cell. The size of the first generation in the calculations was equal to 65 structures. 60% of the structures with the lowest enthalpy were selected after the optimization and then used for the production of the next generation. A new generation was produced as follow: 35% of all structures were generated by heredity, 20% — by atomic mutation, 10% — by lattice permutation, and 35% — randomly. In average 38–44 generations have been produced and relaxed at each pressure. Using AIRSS about 4000–4200 structures were randomly generated and optimized at 50 GPa, and those with the lowest enthalpy were selected.

The total energies and forces were calculated by solving the Schrödinger equation based on projector augmented planewave implementation of density

*Electronic address:gavryushkin@igm.nsc.ru, p.gavryushkin@g.nsu.ru; Corresponding author

functional theory using VASP package [1, 2]. Exchange correlation effects were treated in the generalized gradient approximation (GGA) with Perdew-Bürke-Ernzerhof scheme [3]. Pseudopotentials with $2p^6 3s^2$(Mg_sv), $2s^2 2p^2$ (C), and $2s^2 2p^4$ (O) electrons have been used.

In all crystal structure prediction calculations, medium-quality optimization was performed using the conjugate gradient. The medium quality settings were as follows: plane-wave cutoff energy — 420 eV; Monkhorst-Pack k-point sampling grid of spacing — 0.5 $Å^{-1}$; Gaussian smearing with parameter σ = 0.2 eV. The most promising predicted structures were then optimized at various pressures with higher accuracy: the cutoff energy — 600 eV, k-point sampling grid of spacing — 0.25 $Å^{-1}$, and σ = 0.1 eV.

Thermodynamic properties. Phonon dispersions and free energy calculations were performed using the Phonopy package [4]. Real-space force constants were calculated using supercell method and finite-displacement method, with a 2×2×2 supercell for MgO, $MgCO_3$-$R\bar{3}c$, and Mg_2CO_4-$Pnma$, 1×1×1 for $MgCO_3$-$C2/m$, and 2×2×1 for Mg_2CO_4-$P2_1/c$. Helmholtz free energies were computed at 8 volumes (starting from 0 GPa to 150 GPa) for MgO and $MgCO_3$-$R\bar{3}c$, at 6 volumes (50–150 GPa) for $MgCO_3$-$C2/m$, at 7 volumes (15–150 GPa) for Mg_2CO_4-$Pnma$, and at 7 volumes (40–150 GPa) for Mg_2CO_4-$P2_1/c$, then corrected for thermal expansion using the quasi-harmonic approximation, resulting in Gibbs free energies in both pressure regimes. In this case, high quality settings were used: the cutoff energy — 800 eV, k-point sampling grid of spacing — 0.2 $Å^{-1}$, and σ = 0.05 eV.

Melting temperature. We perform ab intio molecular dynamic simulations to determine the melting curve using *Z-method* [5], which has been proven successful to predict melting temperature in several systems. The pseudopotentials for Mg, C, and O were the same as in the crystal structure prediction calculations. We used plane-wave cutoff of 450 eV, and the Brillouin zone was sampled only with the Γ point. Simulations were performed in the NVE ensemble, using supercell of Mg_2CO_4-$Pnma$ with 224 atoms, for two volumes of 57.465 and 60.982 $Å^3$/f.u. For each volume the system was simulated for 10000–14000 steps with the time step of 1.0 fs for different initial kinetic energy in order to construct an isochoric curve T vs P.

Elastic properties. The elastic constants C_{ij} were evaluated using the stress-strain method $\sigma_i = C_{ij}\epsilon_j$. Four different strains (±0.01 and ±0.02) were applied in each distortion and the resulting stress-strain values were then fitted. Obtained elastic constants then used to calculate the elastic moduli. In order to compute elastic moduli, we apply the Voigt–Reuss–Hill approximation [6,7]. In this approach, the actual effective modulus for a system is approximated by the arithmetic mean of the two well-known bounds for single-crystals according to Voigt [8] and Reuss [9]. The mathematical formulation is provided below.

For $MgCO_3$-$R\bar{3}c$:

$$
\begin{aligned}
B_V &= \frac{1}{9}\big[2(C_{11}+C_{12})+4C_{13}+C_{33}\big],\\
B_R &= \frac{C^2}{M},\\
B &= B_{VRH} = \frac{B_V+B_R}{2}.
\end{aligned}
$$

$$
\begin{aligned}
G_V &= \frac{1}{30}(M+12C_{44}+12C_{66}),\\
G_R &= \frac{5}{2}\left[\frac{C^2C_{44}C_{66}}{3B_VC_{44}C_{66}+C^2(C_{44}+C_{66})}\right],\\
G &= G_{VRH} = \frac{G_V+G_R}{2},
\end{aligned}
$$

where

$$
\begin{aligned}
M &= C_{11}+C_{12}+2C_{33}-4C_{13}^2,\\
C^2 &= (C_{11}+C_{12})C_{33}-2C_{13}^2.
\end{aligned}
$$

For Mg_2CO_4-$Pnma$:

$$
\begin{aligned}
B_V &= \frac{1}{9}\big[C_{11}+C_{22}+C_{33}+2(C_{12}+C_{13}+C_{23})\big],\\
B_R &= \Delta\big[C_{11}(C_{22}+C_{33}-C_{23})+C_{22}(C_{33}-2C_{13})-2C_{33}C_{12}+C_{12}(2C_{23}-C_{12})\\
&\quad +C_{13}(2C_{12}-C_{13})+C_{23}(2C_{13}-C_{23})\big]^{-1},\\
B &= B_{VRH} = \frac{B_V+B_R}{2}.
\end{aligned}
$$

$$
\begin{aligned}
G_V &= \frac{1}{15}\big[C_{11}+C_{22}+C_{33}+3(C_{44}+C_{55}+C_{66})-(C_{12}+C_{13}+C_{23})\big],\\
G_R &= 15\Big\{4\big[C_{11}(C_{22}+C_{33}+C_{23})+C_{22}(C_{33}+C_{13})+C_{33}C_{12}-C_{12}(C_{23}+C_{12})\\
&\quad -C_{13}(C_{12}+C_{13})-C_{23}(C_{13}+C_{23})\big]/\Delta+3\big[\frac{1}{C_{44}}+\frac{1}{C_{55}}+\frac{1}{C_{66}}\big]\Big\}^{-1},\\
G &= G_{VRH} = \frac{G_V+G_R}{2},
\end{aligned}
$$

where

$$
\Delta = C_{13}(C_{12}C_{23}+C_{13}C_{22})+C_{23}(C_{12}C_{13}-C_{23}C_{11})+C_{33}(C_{11}C_{22}-C_{12}^2).
$$

In the following formulas, subscript V denotes the Voigt bound, R denotes the Reuss bound, and VRH denotes the Voigt–Reuss–Hill average.

The isotropic wave propagation velocities in the material can then be evaluated from the bulk and shear moduli and the density, ρ, as follows

$$V_p = \sqrt{\frac{B + \frac{4}{3}G}{\rho}}, \qquad V_s = \sqrt{\frac{G}{\rho}}.$$

There are many descriptions of anisotropy named the compression anisotropy (A_B) and the shear anisotropy (A_G) which represent the percentage of the bulk modulus and shear modulus, correspondingly, and the universal anisotropy index. They can be obtained as follows:

$$\begin{aligned} A_B &= \frac{B_V - B_R}{B_V + B_R}, \\ A_G &= \frac{G_V - G_R}{G_V + G_R}, \\ A^U &= 5\frac{G_V}{G_R} + \frac{B_V}{B_R} - 6. \end{aligned}$$

If A_B, A_G, and A^U are equal to zero, phase turns to isotropic crystal. A_B and A_G could vary from 0 to 1 (i.e from 0 to 100 % anisotropy).

Results

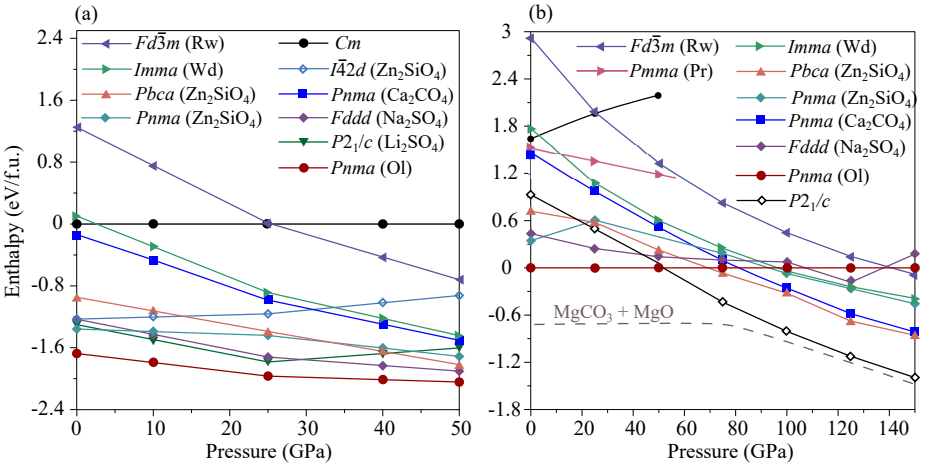

Figure S1: Enthalpy-pressure dependencies of the predicted Mg_2CO_4 structures in the pressure range 0–50 GPa (a) and 0–150 GPa (b). The grey dashed line represent relative enthalpy of the ($MgCO_3$+MgO) mixture. In legend, isostructural compounds are indicated in brackets: Rw – ringwoodite, Wd – wadsleyite, Pr – poirierite, Ol – olivine

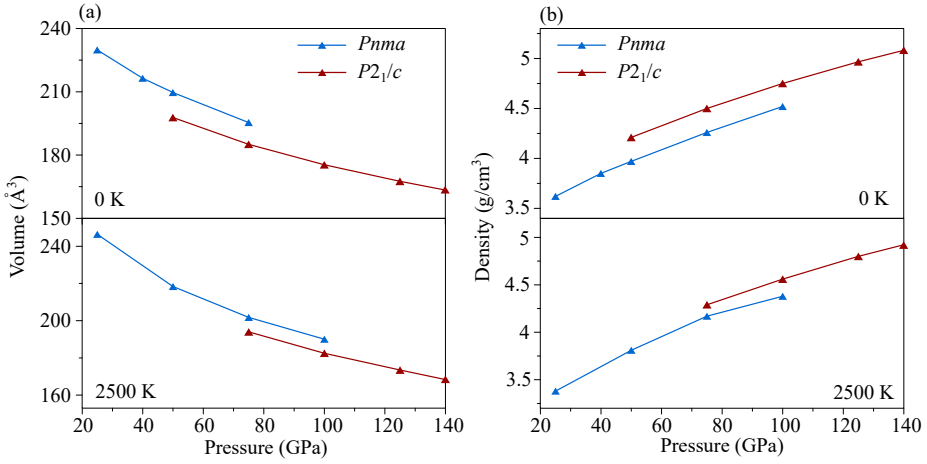

Figure S2: Volume (a) and density (b) dependencies of pressure for Mg-orthocarbonate.

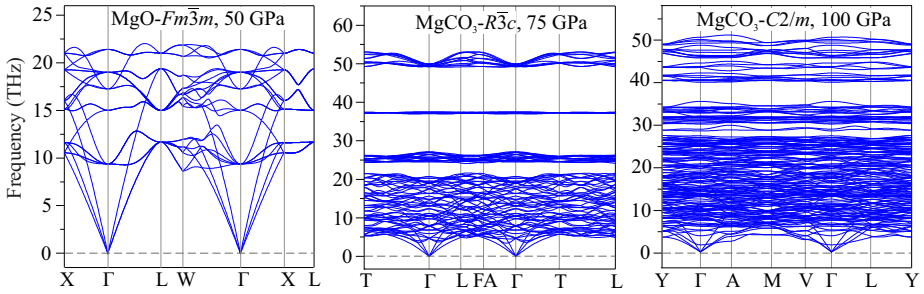

Figure S3: Phonon dispersion curves of MgO at 50 GPa, $MgCO_3$-$R\bar{3}c$ at 75 GPa, and $MgCO_3$-$C2/m$ at 100 GPa.

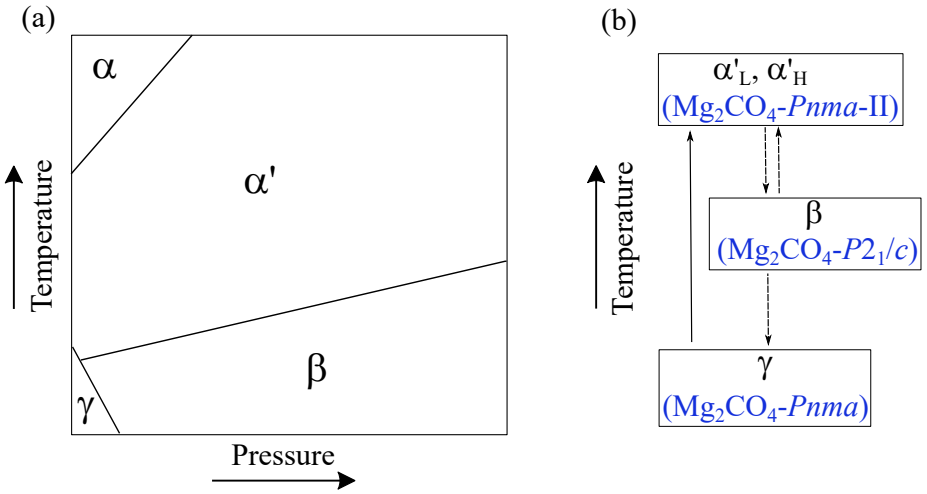

Figure S4: Schematic $P-T$ phase diagram of Ca_2SiO_4 according to [10] (a) and corresponding sequences of phase transitions realised on heating at ambient pressure (b). Dashed line corresponds to metastable phase transitions, solid line — to stable transitions.

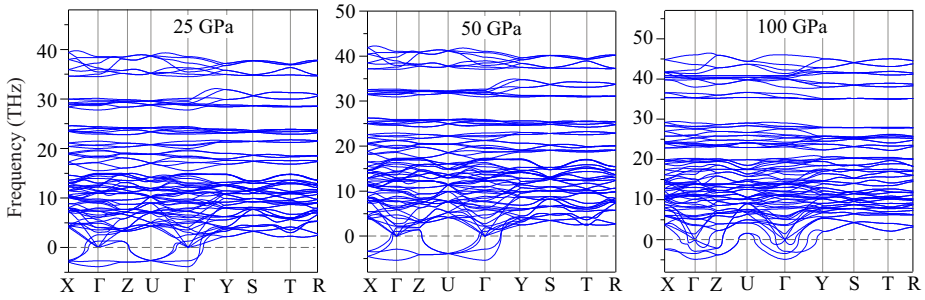

Figure S5: Phonon dispersion curves for dynamically unstable phase of magnesium orthocarbonate, Mg_2CO_4-*Pnma*-II at 25 GPa, 50 GPa, and 100 GPa.

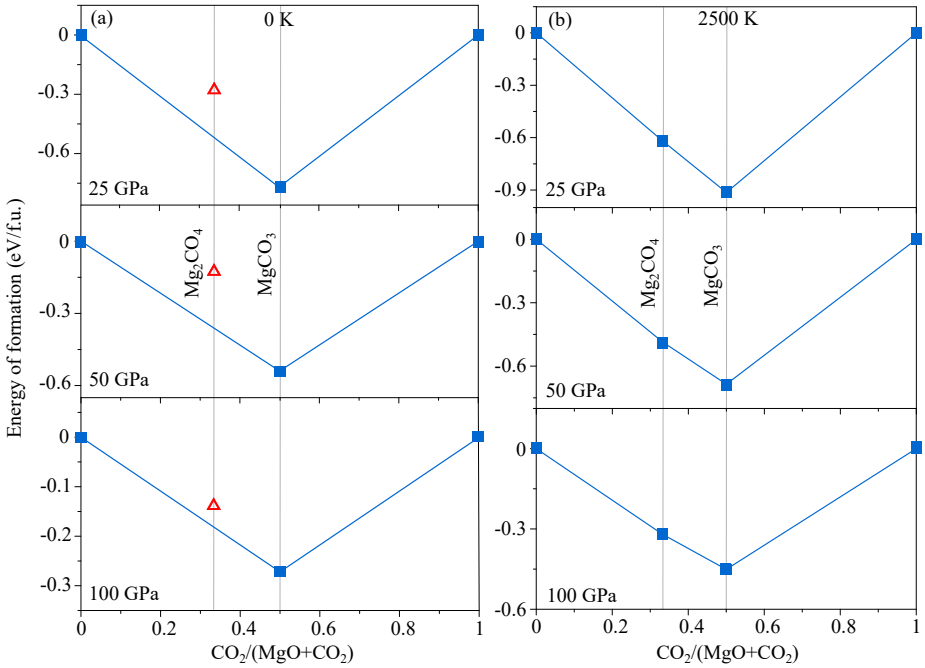

Figure S6: Thermodynamic convex hulls for MgO-CO_2 system at 0 GPa, 50 GPa, and 100 GPa and 0 K (a) and 2500 K (b). Blue filled squares denote stable structures, and red open triangles — metastable ones.

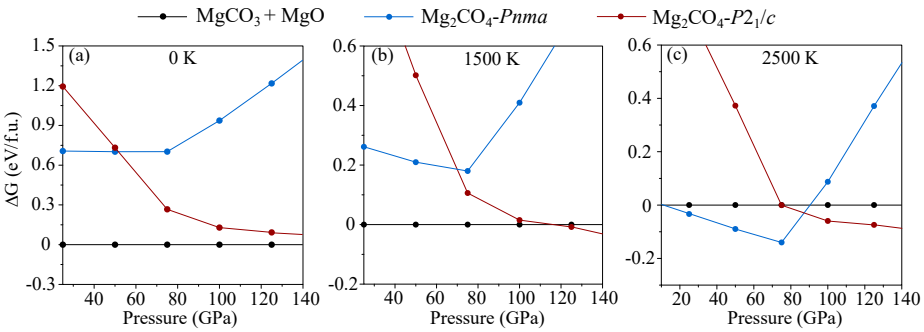

Figure S7: The relative Gibbs free energies as function of pressure for Mg_2CO_4=$MgCO_3$+MgO reaction at 0 K (a), 1500 K (b), and 2500 K (c).

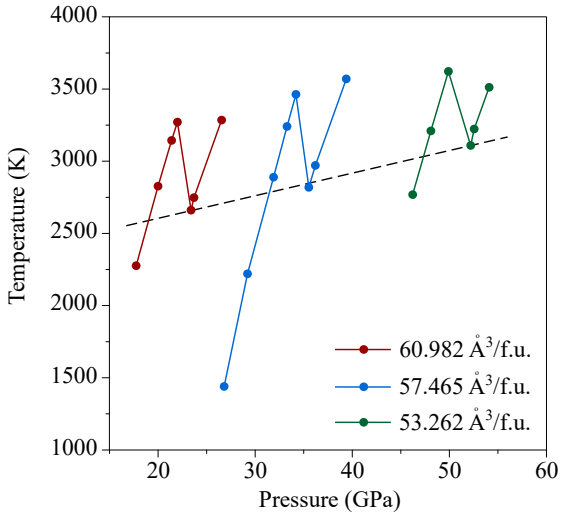

Figure S8: The Z isochores for Mg_2CO_4-$Pnma$ at volumes 53.252 Å^3/f.u., 57.465 Å^3/f.u. and 60.982 Å^3/f.u. shown by blue and red lines, respectively.

Table S1: Calculated elastic constants C_{ij} (GPa) of $MgCO_3$-$R\bar{3}c$ and Mg_2CO_4-$Pnma$ at 50 GPa and 0 K.

Phase	C_{11}	C_{12}	C_{13}	C_{22}	C_{23}	C_{33}	C_{44}	C_{55}	C_{66}
Mg_2CO_4-$Pnma$	375.9	272.6	234.5	497	253.4	572.9	170.6	161.3	124.4
$MgCO_3$-$R\bar{3}c$	543.9	239.5	230.6	543.9	230.6	352.4	122.4	122.4	152.3

Table S2: Calculated density ρ (kg/m^3), bulk modulus B (GPa), shear modulus G (GPa), compression V_p (km/s) and shear V_s (km/s) velocities, compression anisotropy A_B, shear anisotropy A_G, and universal anisotropy A^U indexes of Mg_2CO_4-$Pnma$ and $MgCO_3$-$R\bar{3}c$ at 50 GPa and 0 K.

Phase	ρ	B	G	V_p	V_s	A_B	A_G	A^U
Mg_2CO_4-$Pnma$	3951.72	324.3	131.3	11.24	5.77	0.0165	0.0425	0.4772
$MgCO_3$-$R\bar{3}c$	3798.67	307.8	125.9	11.19	5.76	0.0256	0.0226	0.2838

References

[1] Kresse, G.; Furthmüller, J. Efficient iterative schemes for ab initio total-energy calculations using a plane-wave basis set. *Phyical Review B 54*, **1996**, 11169–11186.

[2] Kresse, G.; Furthmüller, J. Efficiency of ab-initio total energy calculations for metals and semiconductors using a plane-wave basis set. *Computational Materials Science 6*, **1996**, 15 – 50.

[3] Perdew, J. P.; Burke, K.; Ernzerhof, M. Generalized gradient approximation made simple. *Physical Review Letters 77*, **1996**, 3865–3868.

[4] Togo, A.; Tanaka, I. First principles phonon calculations in materials science. *Scripta Materialia 108*, **2015**, 1–5.

[5] Belonoshko, A. B.; Skorodumova, N. V.; Rosengren, A.; Johansson, B. Melting and critical superheating. *Physical Review B 73*, **2006**, 012201.

[6] Hill, R. The elastic behaviour of a crystalline aggregate. *Proceedings of the Physical Society. Section A 65*, **1952**, 349–354.

[7] Hill, R. Elastic properties of reinforced solids: Some theoretical principles. *Journal of the Mechanics and Physics of Solids 11*, **1963**, 357 – 372.

[8] Voigt, W. Lehrbuch der kristallphysik (textbook of crystal physics). *BG Teubner, Leipzig und Berlin* **1928**.

[9] Reuss, A. Calculation of the flow limit of solid solution based on the plasticity condition for single crystals. *ZAMM-Journal of Applied Mathematics and Mechanics / Zeitschrift für Applied Mathematics and Mechanics 9*, **1929**, 49–58.

[10] Belmonte, D.; Ottonello, G.; Zuccolini, M. V. Ab initio-assisted assessment of the CaO-SiO_2 system under pressure. *Calphad 59*, **2017**, 12 – 30.